Available online at www.sciencedirect.com
ScienceDirect
Remote Sensing of Environment 106 (2007) 508–524
Remote Sensing of Environment
www.elsevier.com/locate/rse

Detecting induced *in situ* erodibility of a dust-producing playa in Australia using a bi-directional soil spectral reflectance model

Adrian Chappell [a,*], Craig Strong [b], Grant McTainsh [b], John Leys [c]

[a] *Centre for Environmental Systems Research, School of Environment and Life Sciences, University of Salford, Manchester, M5 4WT, UK*
[b] *Desert Knowledge Cooperative Research Centre, Faculty of Environmental Sciences, Griffith University, Brisbane, Queensland, 4111, Australia*
[c] *Department of Natural Resources, Far West Region Science and Information Branch, Gunnedah, NSW 2380, Australia*

Received 8 August 2006; received in revised form 15 September 2006; accepted 16 September 2006

Abstract

Two sites on a playa (claypan) in south western Queensland, Australia were chosen to represent the variability in soil surface conditions known to control wind erosion and dust production in the region. The material was very fine and comprised of large amounts and different types of salts, high electrical conductivity, a propensity for slaking and the presence of cyanobacteria. The surfaces of 4 plots at each site were modified using *in situ* rainfall simulation and wind tunnel abrasion. The changes in the surface conditions were recorded using digital images and multi-angular spectral measurements of reflectance and inverted against a soil bi-directional spectral reflectance model. Optimised values of the model parameters produced the single scattering albedo (SSA) and a description of the scattering behaviour of the soil surfaces that included an estimate of microscopic roughness. The model parameters removed the effect of the measurement conditions (illumination and viewing geometry) on the spectral reflectance.

Abrasion of the untreated surfaces demonstrated that the variability in the antecedent surface conditions played an important role in their response. Rainfall, drying and subsequent abrasion appeared to reset the soil surface conditions and controlled the spatial and temporal variation in the soil surface conditions. Redundancy analyses, conducted separately for SSA of selected wavebands, model parameter values and treatments elucidated the subtle and interactive effects of the treatments and surface responses. The results showed that high intensity rainfall and abrasion was associated with wavebands in the visible region and reduced roughness. Low intensity rainfall was associated with wavebands in the near-infrared and short-wave infrared regions and increased roughness. The analysis was interpreted as the result of eluviation due to rainsplash impact which caused size segregation and the preferential translocation of iron oxides to the surface and the creation of a thick surface seal and caused a thin crust which enabled the movement of salts and/or mineral clays to the surface because of the strong evaporation gradient. A poor relationship between aerodynamic resistance and microscopic roughness suggested that features of soil surface erodibility created by natural environmental processes such as rainsplash and wind erosion required a correction for macroscopic roughness. The values of the model parameters appeared to be insensitive to the directional nature of the abrasion process. The findings are significant for the development of this work towards an airborne or satellite-based assessment of soil surface erodibility and erosion.

Keywords: Wind erosion; Aerodynamic resistance; Soil erodibility; Cyanobacteria; Soil crust; Roughness; Playa; Wind tunnel; Rainfall simulator; Soil bi-directional spectral reflectance model; Canonical ordination; Redundancy analysis

1. Introduction

Recent developments in wind erosion models (e.g., Böhner et al., 2003; Fryrear et al., 1998; Shao & Leslie, 1997) and models of dust emission (e.g., Marticorena & Bergametti, 1995; Sokolik & Toon, 1996; Zender et al., 2003) have emphasised the need for information on the spatial and temporal variation of soil surface composition and structure, because they control the susceptibility of soil to wind erosion (erodibility) and hence the emission of dust (Zobeck, 1991b). Shao et al. (1996) suggested that the main limitation of wind erosion models is their inability to incorporate the evolution of surface soil conditions. The wind erosion prediction system (WEPS) is a sophisticated example of how the dynamic behaviour of a soil surface may be incorporated. However, it requires a considerable amount of

* Corresponding author.
E-mail address: a.chappell@salford.ac.uk (A. Chappell).

0034-4257/$ - see front matter © 2006 Elsevier Inc. All rights reserved.
doi:10.1016/j.rse.2006.09.009

information about the behaviour of the soil, micro-climate etc. that renders the model very difficult to apply across large areas and across several scales of variation, regardless of the nature of those scales. The field data collected are often limited in space and time and sampling is intrusive to the soil surface making it difficult to appreciate the simultaneous evolution of the surface in space and time. Shao et al. (1996) provided one of the first physically-based wind erosion models to operate across spatial scales; from the field to the continent (Australia). Shao and Leslie (1997) suggested that the Shao et al. (1996) model required more detailed estimation of erodibility, in particular the estimation of surface roughness elements, soil water content and surface crusting. Nevertheless, one of the main reasons for the success of the Shao model was its inclusion of remote sensing data (to approximate frontal area index of non-erodible roughness elements using NDVI data). Remote sensing of soils has been demonstrated to have considerable potential for the assessment of soil erodibility and soil erosion (Baumgardner et al., 1985; Ben-Dor et al., 1999; Huete & Escadafal, 1991; Latz et al., 1984; Seubert et al., 1979; Stoner & Baumgardner, 1981). There appear to be two requirements for large area assessment of soil erodibility (Chappell et al., 2005): a) that a holistic conceptual framework is used to describe how the factors of erodibility operate in a time-space continuum (Geeves et al., 2000), and b) that a measurement technique is used that can provide high resolution spatio-temporal data to characterise this time-space continuum.

The multi-angular measurement of spectral reflectance appears to meet these requirements by providing a single framework within which changes at the soil surface can be considered (Chappell et al., 2006). Although this framework appears to lend itself to multi-scale assessments across large areas using existing and forthcoming generations of angular sensors on airborne and satellite platforms there are many issues which must be addressed before this ambitious goal can be reached. Chappell et al. (2006) used rainfall simulation and wind tunnel abrasion to demonstrate that multi-angular measurements and a bi-directional soil spectral reflectance model can be used to examine soil surface erodibility. However, the removal of soil from its environment inevitably disturbs its natural condition, therefore in-field measurement is preferable (Pinty et al., 1989). Such measurements should be accompanied by measurements of the soil surface and natural environmental processes operating at the time. This is practically difficult to achieve, especially in regions where the spatial and temporal variation in soil surface conditions is large. This difficulty was overcome by inducing the main environmental processes (rainfall and wind erosion) and making *in situ* multi-angular spectral reflectance measurements of soil surfaces.

The aim of the present study is to examine under controlled conditions the extent to which a bi-directional soil spectral reflectance model (Jacquemoud et al., 1992) can retrieve information about the *in situ* soil surface condition after predetermined treatments. To reduce complexity as much as possible for this experiment a playa (claypan) was chosen for the experiment. Topographic lows are recognised as being one of the most important sources of global dust emission within drylands (e.g., Mahowald et al., 2003). The playa study area in Australia is well known for its wind erosion and dust production. The environment has very little vegetation and is relatively homogeneous with respect to the type of material but is diverse in terms of soil surface conditions. The study provided a further opportunity to move closer to the larger research goal of using the single framework of multi-angular spectral reflectance to integrate the assessment of soil surface composition and structure and consider the concept of erodibility on a continuum in terms of its spatial and temporal variation. Ultimately, the intention is to develop a soil erosion model around a soil bi-directional spectral reflectance model.

2. Methods

2.1. Study area

The study area is the Lake Constance claypan (or playa) on the high floodplain of the anastomosing Diamantina River (Fig. 1) in Diamantina National Park (DNP), western Queensland, Australia. The claypan is approximately 5 km × 5 km and is bordered by red sand dunes on the northeast and southwest (Fig. 1). The playa lies within a currently active aeolian transport region (Nickling et al., 1999) and has been the focus of a number of wind erosion experiments by the authors (e.g., Chappell et al., 2003a,b; McTainsh et al., 1999). During floods large quantities of fine grained alluvium are deposited on the floodplain that is subsequently remobilised by aeolian activity (McTainsh et al., 1999). The mean annual rainfall for the region is approximately 270 mm and the last flood to inundate the claypan was February 2000.

During this study (August and September, 2002) the playa was largely bare with few areas of plant cover. The playa soil was a brown Vertosol with surface alluvial and aeolian deposits. Unconsolidated material on the sealed surface formed a fine sandy veneer derived from alluvial deposition and near the playa margins dunes provided coarser red sands. Despite its propensity for slaking, the playa surface had a complex continuum of surface conditions that varied in thickness, strength and porosity, from extremely loose, aerated and fragile to thick, massive and hard packed. Two sites of bare soil on the playa were chosen to represent the variation in the continuum of surface conditions and therefore in the erodibility. Table 1 provides some of the soil properties at those sites.

2.2. Soil treatments

A portable field wind tunnel and rainfall simulator were transported to the sites and used to reproduce aeolian abrasion and rainfall under controlled conditions. At each site, four plots were located for applying the various treatments. Table 2 summarises the activity on each plot and at each site. While it is common to provide replicates of treatments so that uncertainty in the results might be considered (e.g., Chappell et al., 2006), the large variability in space and time of wind erosion and soil erodibility (Chappell et al., 2003a,b) meant that plots could not reliably be used as replicates. Instead, they were used to

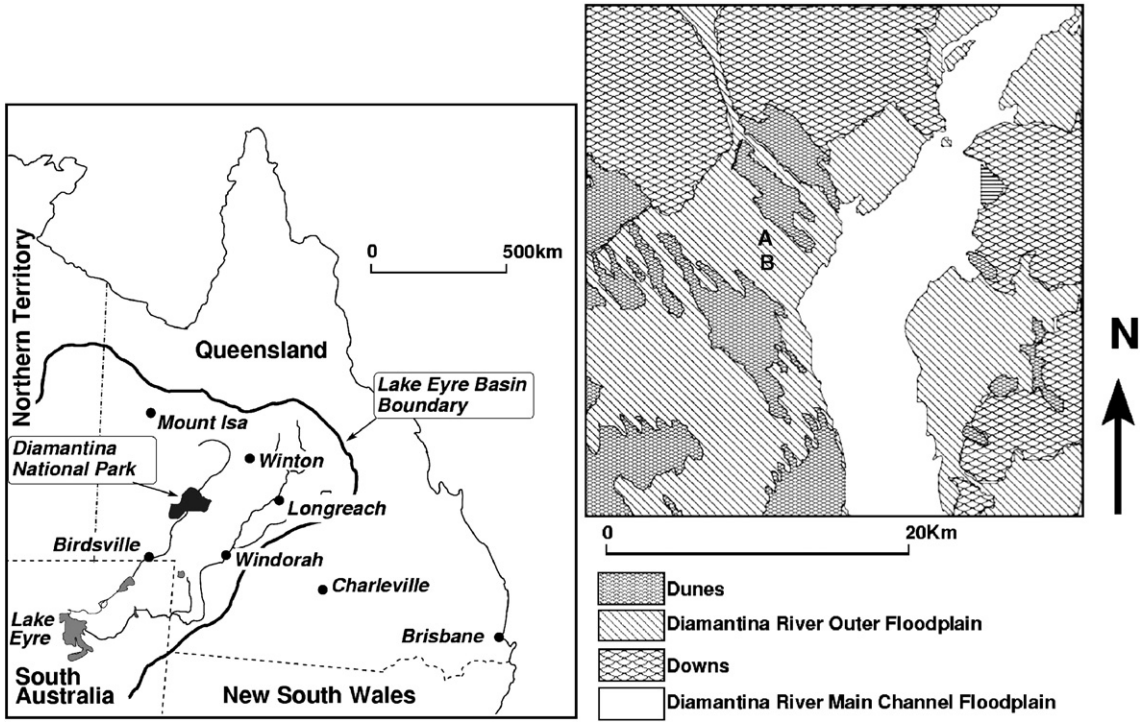

Fig. 1. The location of the Lake Constance claypan in the Diamantina National Park study area in western Queensland, eastern Australia and a representation of the study area showing the location of the experimental sites (A and B), the orientation of dunes and the nearest branch of the anastomosing river Diamantina (modified from Butler et al., 2005).

consider the response to different combinations and intensities of the simulations (Table 2).

The plots at each site were orientated differently to ensure that the orientation of the wind tunnel was always perpendicular to the prevailing wind direction (to reduce the influence of pressure fluctuations). The plots at site A were orientated northeast (i.e., 40° east of north) and at site B they were orientated south (i.e., 174° east) (Fig. 2).

2.3. Wind erosion simulation

The wind tunnel was of the blowing type and details of its construction are described by Leys and Raupach (1991). An array of pitot tubes was used to construct the wind velocity profile and to estimate the aerodynamic resistance of the surface roughness using the roughness length (z_0) in the same manner as that described by Dong et al. (2002). A vertically integrated (Modified Bagnold trap; Shao et al., 1993) was located 1 m from the end of the tunnel. The wind tunnel was operated for 30 min constantly at 14 m s^{-1} (measured at 0.3 m height). During the first minute of operation no abrader sand was added to the air stream (in an attempt to sample only the loose erodible material from the surface). Thereafter, abrader sand was added at a constant rate (19±2 g m^{-1} s^{-1}). Combined samples of the abrader sand and soil surface emissions were trapped at the outlet of the tunnel every minute for the first 5 min and then every 5 min; providing a total of 10 samples.

Table 1
Some characteristics of the playa soil (0–10 cm) at the sites (A and B) used in the experiments

	A	B
UTM x	501069	500519
UTM y	7370805	7372447
Clay (%)	43.89	38.36
Silt (%)	23.11	25.64
Fine sand (%)	32.67	35.54
Ec1:5 (ds/m)	0.90	0.50
Cl (mg/kg)	1756.99	3969.81
Na (mg/kg)	853.38	1340.93
CEC (mg/kg)	21.29	22.62
Mg (mg/kg)	4.72	7.09
Ca (Mg/kg)	11.16	11.87
K (mg/kg)	0.75	0.24
Fe (%)	1.07	0.60

2.4. Rainfall simulation

A rotating-disc rainfall simulator (Morin et al., 1967) was used to deliver rain drops to the plot surfaces over a period of 5 min. Local rainfall conditions typical of thunderstorms and gentle rain were simulated at rainfall rates of 110 mm h^{-1} or 45 mm h^{-1} respectively, and locally-collected rain water was used. The simulations were designed to produce two surface wetness conditions: a ponded surface and a moist soil surface. Continuous operation of the rainfall simulator for 5 min at 110 mm h^{-1} or 45 mm h^{-1} created ponding at the surface, henceforth referred to as high and low intensity ponding rainfall (*R110P* and *R45P*, respectively). In other treatments, ponding of water at the surface was avoided by the discontinuous application of rainfall with an increasing delay between applications. In this case, the rainfall simulator was operated at 110 mm h^{-1} or 45 mm h^{-1} for a total of 5 min, but with a

Table 2
Indicators of locations, plots and treatments for samples used as 'environmental' variables for redundancy analysis

	Site		Plots				Treatments								
Sample	A	B	1	2	3	4	A1	A1	R1	R2	R3	R3	R4	R4	PH
110	1	0	1	0	0	0	0	0	0	0	0	0	0	0	0
111	1	0	1	0	0	0	1	0	0	0	0	0	0	0	0
112	1	0	1	0	0	0	1	0	1	0	0	0	0	0	0
113	1	0	1	0	0	0	1	1	1	0	0	0	0	0	0
114	1	0	1	0	0	0	1	1	1	0	1	0	0	0	0
115	1	0	1	0	0	0	1	1	1	0	1	0	0	0	1
120	1	0	0	1	0	0	0	0	0	0	0	0	0	0	0
121	1	0	0	1	0	0	1	0	0	0	0	0	0	0	0
122	1	0	0	1	0	0	1	0	0	1	0	0	0	0	0
123	1	0	0	1	0	0	1	1	0	1	0	0	0	0	0
124	1	0	0	1	0	0	1	1	0	1	0	0	1	0	0
125	1	0	0	1	0	0	1	1	0	1	0	0	1	0	1
130	1	0	0	0	1	0	0	0	0	0	0	0	0	0	0
131	1	0	0	0	1	0	0	0	0	0	1	0	0	0	0
132	1	0	0	0	1	0	1	0	0	0	1	0	0	0	0
133	1	0	0	0	1	0	1	0	0	0	1	1	0	0	0
135	1	0	0	0	1	0	1	0	0	0	1	1	0	0	1
140	1	0	0	0	0	1	0	0	0	0	0	0	0	0	0
141	1	0	0	0	0	1	0	0	0	0	0	0	1	0	0
142	1	0	0	0	0	1	1	0	0	0	0	0	1	0	0
143	1	0	0	0	0	1	1	0	0	0	0	0	1	1	0
144	1	0	0	0	0	1	1	1	0	0	0	0	1	1	0
145	1	0	0	0	0	1	1	1	0	0	0	0	1	1	1
210	0	1	1	0	0	0	0	0	0	0	0	0	0	0	0
211	0	1	1	0	0	0	1	0	0	0	0	0	0	0	0
212	0	1	1	0	0	0	1	0	1	0	0	0	0	0	1
220	0	1	0	1	0	0	0	0	0	0	0	0	0	0	0
221	0	1	0	1	0	0	1	0	0	0	0	0	0	0	0
222	0	1	0	1	0	0	1	0	0	1	0	0	0	0	1
230	0	1	0	0	1	0	0	0	0	0	0	0	0	0	0
231	0	1	0	0	1	0	0	0	0	0	1	0	0	0	0
232	0	1	0	0	1	0	1	0	0	0	1	0	0	0	1
240	0	1	0	0	0	1	0	0	0	0	0	0	0	0	0
241	0	1	0	0	0	1	0	0	0	0	0	0	1	0	0
242	0	1	0	0	0	1	1	0	0	0	0	0	1	0	1

A1 = Wind tunnel operated for 30 min at 14 m s-1 (at 30 cm height) with 19 g m^{-1} s^{-1}.
R1 = Rainfall simulator set at 110 mm h^{-1} and operated discontinuously for 5 min at 1 min intervals with increasing delays between simulations (i.e., 2, 4, 8 and 16 min delays).
R2 = Rainfall simulator set at 45 mm h^{-1} and operated discontinuously for 5 min at 1 min intervals but with increasing delays between simulations (i.e., 2, 4, 8 and 16 min delays).
R3 = Rainfall simulator set at 110 mm h^{-1} and operated continuously for 5 min.
R4 = Rainfall simulator set at 45 mm h^{-1} and operated continuously for 5 min.
PH = Breakdown in the radiometric equipment curtailed the experiments and allowed undefined natural environmental processes to act on the surface before the reflectance was repeated (post-hiatus).

delay of 2, 4, 8 and 16 min between each application. These treatments are henceforth referred to as high and low intensity non-ponding rainfall (*R110NP* and *R45NP*, respectively).

Since clay soils with variable soil moisture are known to have an adverse effect on the retrieval of the bi-directional reflectance parameters (see following section) each plot was allowed to dry naturally for at least 48 h after rainfall simulation. The clear skies and slightly windy conditions during the fieldwork ensured highly evaporative conditions that dried rapidly the soil surface and ensured that the soil surface moisture was consistently small during the bi-directional reflectance measurements.

2.5. Bi-directional reflectance model and its application

Pinty et al. (1989) extended the work of Hapke (1963, 1981) to describe the range of soil surfaces on Earth where individual particles have non-uniform angular distributions. Jacquemoud et al. (1992) extended the model to explain backward and forward scattering (the specular effect) of light by smooth soils of different types. This model and its parameters were useful for characterising prepared soil surfaces and changes to them induced by laboratory rainfall simulation and wind tunnel abrasion (Chappell et al., 2006). It is also used here because of its appropriateness to the smooth playa soils. The parameters of the model include: (i) the single scattering albedo (ω) (SSA is the ratio of the scattered energy to the total energy either scattered or absorbed by the particle), (ii) a roughness parameter (h) (which appears to be related to: particle size distribution, porosity and the gradient of compaction with depth (Hapke, 1963) and is caused by small shadows behind individual particles and micro-aggregates (Cierniewski, 1987)). The remaining four parameters (b, c, b' and c') are diagnostic of the type of scattering of light and have been demonstrated by Jacquemoud et al. (1992; p. 125), and used by Chappell et al. (2006), to identify backscattering (towards the direction of illumination) and forward scattering (away from the direction of illumination) and mixed scattering (backwards and forwards relative to the direction of illumination). The retrieved values should depend on the soil surface condition, not the illumination and viewing geometry. Jacquemoud et al. (1992) concluded that the retrieved parameters were invariant for a given soil, except for smooth soils with a large clay content, which exhibited a large specular effect near soil moisture saturation, but with a decreased specular effect and increased backscatter with drying.

Since the radiometric properties of a bare soil surface can be described by the model of Jacquemoud et al. (1992) the challenge is to find the values of the six parameters such that the computed value of the reflectance best approximates the actual observations. Following Pinty et al. (1989) and Jacquemoud et al. (1992) a non-linear least squares fitting procedure was

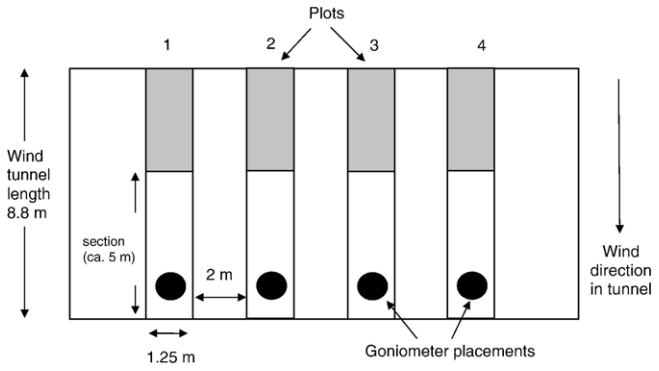

Fig. 2. Schematic representation of the experimental plots at each of the two sites (A and B) in the study area (not to scale).

A

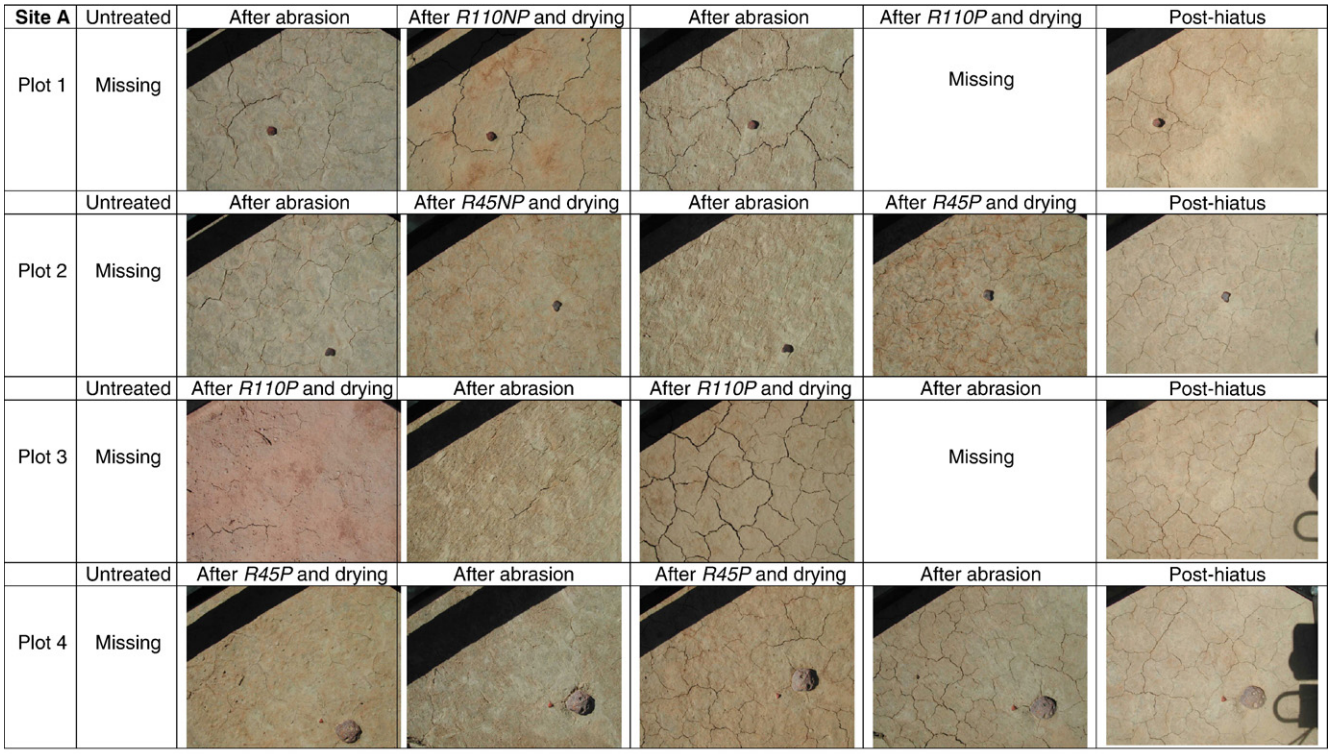

B

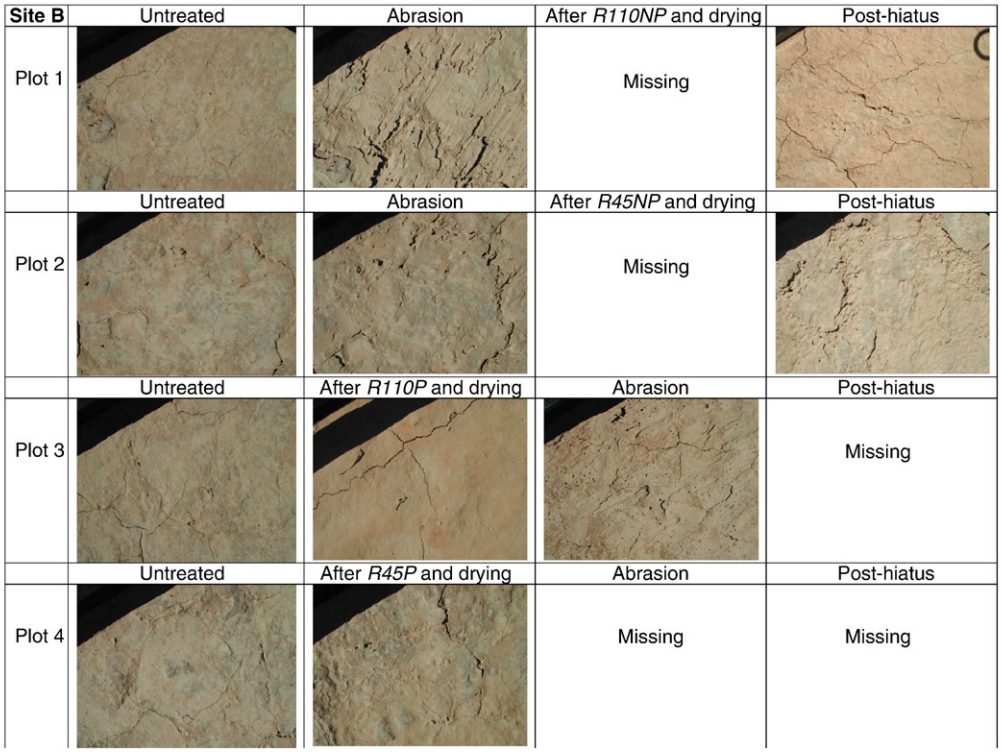

Fig. 3. On-nadir digital photographs (1000×750 pixels) taken before and after treatment (see text for details) at site A (A) and site B (B). Note that the azimuth orientation does not remain the same within and between plots.

used to solve that inverse problem. Details of the approach can be found in those original papers and the practical implementation and sensitivity of the approach used here is the same as that described by Chappell et al. (2006).

2.6. Angular spectral reflectance measurements

The Analytical Spectral Devices (ASD) spectroradiometer used here had a spectral range of 350–2500 nm and spectral

Table 3
Optimised values for the parameters from Jacquemoud et al. (1992) bi-directional soil spectral reflectance model of the treatments applied to each plot at two sites

			Bi-directional reflectance model parameters					
Sample	Site	Treatment	*b*	c	h	b′	*c′*	RMSE
110	A	Untreated	−0.06	0.47	8.15	0.86	−0.05	0.02
111	A	Abrasion	0.93	−0.36	4.34	0.95	0.01	0.02
112	A	*R110NP*	1.74	−0.62	5.35	−0.04	0.43	0.02
113	A	Abrasion	0.63	−0.64	4.34	0.82	0.16	0.02
114	A	*R110P*	−0.87	0.37	9.93	−0.81	0.38	0.02
115	A	PH	1.12	−0.49	5.61	1.67	−0.57	0.04
120	A	Untreated	1.26	−0.46	5.82	0.02	0.24	0.01
121	A	Abrasion	0.61	−0.32	4.22	1.01	−0.16	0.02
122	A	*R45NP*	0.05	0.03	8.21	−0.03	0.15	0.01
123	A	Abrasion	−0.60	0.09	9.96	0.89	−0.25	0.02
124	A	*R45P*	1.23	−0.38	3.41	−0.55	0.67	0.02
125	A	PH	0.44	−0.06	7.27	−0.26	0.50	0.01
130	A	Untreated	0.86	−0.41	3.38	1.05	0.01	0.03
131	A	*R110P*	0.62	0.02	8.26	0.72	−0.06	0.01
132	A	Abrasion	0.77	−0.72	3.81	1.05	−0.13	0.01
133	A	*R110P*	0.41	−0.11	2.51	0.42	−0.03	0.02
135	A	PH	1.43	−0.62	1.56	0.08	0.33	0.01
140	A	Untreated	1.45	−0.64	9.60	0.24	0.05	0.03
141	A	*R45P*	2.05	0.93	2.96	0.33	0.14	0.02
142	A	Abrasion	0.89	−0.12	8.48	−0.24	0.76	0.04
143	A	*R45P*	1.23	−0.57	8.46	−0.57	0.63	0.03
144	A	Abrasion	0.70	−0.46	4.27	0.82	0.02	0.02
145	A	PH	0.13	−0.05	0.35	0.69	−0.08	0.02
210	B	Untreated	0.63	−0.23	7.03	0.26	0.13	0.02
211	B	Abrasion	1.23	−0.53	5.22	0.90	0.00	0.02
212	B	*R110NP*+PH	0.05	0.06	8.43	−0.12	0.31	0.02
220	B	Untreated	0.76	−0.43	4.46	1.07	−0.15	0.02
221	B	Abrasion	1.01	−0.59	4.17	1.31	−0.37	0.02
222	B	*R45NP*+PH	1.29	−0.49	5.13	0.37	0.24	0.01
230	B	Untreated	1.02	−0.57	5.05	1.09	−0.20	0.02
231	B	*R110P*	1.30	0.30	9.95	1.11	0.48	0.02
232	B	Abrasion+PH	1.65	−0.75	5.16	0.76	0.16	0.01
240	B	Untreated	1.22	−0.60	5.08	1.43	−0.42	0.03
241	B	*R45P*	2.25	−0.58	6.18	−0.17	1.01	0.04
242	B	Abrasion+PH	1.31	−0.74	4.19	0.53	0.26	0.02

Abrasion=Wind tunnel operated for 30 min at 14 m s-1 (at 30 cm height) with 19 g m^{-1} s^{-1}.
R110NP=Rainfall simulator set at 110 mm h^{-1} and operated discontinuously for 5 min at 1 min intervals with increasing delays between simulations (i.e., 2, 4, 8 and 16 min delays).
R45NP=Rainfall simulator set at 45 mm h^{-1} and operated discontinuously for 5 min at 1 min intervals but with increasing delays between simulations (i.e., 2, 4, 8 and 16 min delays).
R110P=Rainfall simulator set at 110 mm h^{-1} and operated continuously for 5 min.
R45P=Rainfall simulator set at 45 mm h^{-1} and operated continuously for 5 min.
PH=Breakdown in the radiometric equipment curtailed the experiments and allowed undefined natural environmental processes to act on the surface before the reflectance was repeated (post-hiatus).

sampling of 1.4 nm between 350–1050 nm and 2 nm between 1000–2500 nm. An 8° field of view was used. A goniometer allowed repeatable and consistent measurements of multi-angular reflectance of the soil surface and enabled several view zenith and view azimuth angles. The radiometer was mounted 40 cm above the soil surface and had a footprint at nadir of approximately 25 cm^2. The viewing azimuth angle relative to the solar azimuth (0° in the principal plane, 90° and 135°) and the view zenith angle (every 10° between −60° away from the sun and +60° towards the sun) were kept constant during the measurement procedure. Some of the view zenith angles were omitted because of the shadow cast by the goniometer. The angles excluded varied according to measurement time. The time and location of measurement was recorded so that the solar zenith and azimuth angle could be determined retrospectively. The solar zenith angle varied between 20° and 65° depending on the time of measurement. A calibrated Spectralon panel was used to reduce the sensitivity of the processed measurements to the characteristics of the source of illumination. Two Spectralon reflectance reference measurements were made immediately before and after the target measurements under the same conditions as the measurement. Measurements were conducted under clear sky conditions between approximately 1000 and 1600 h local time, each day. Conversion to spectral reflectance was conducted by dividing the reflectance spectra of the soil samples by the spectra of the highly reflecting white Spectralon reference panel.

Since the measurements were performed in the field, reflectance at wavebands between 1350–1470 nm and between 1790–1980 nm were removed from the analysis because they were influenced by atmospheric water vapour. Diffuse irradiance

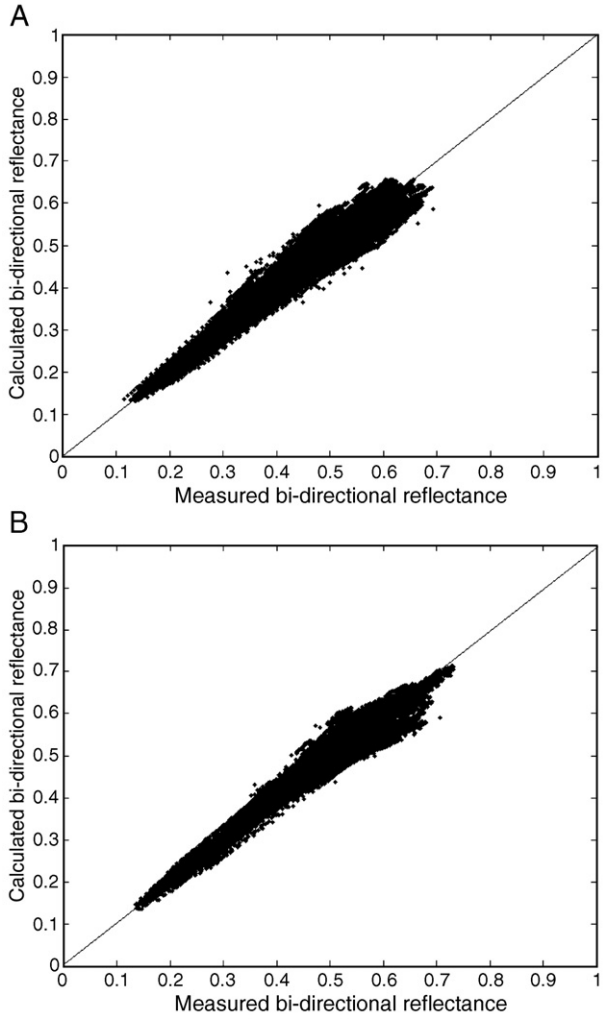

Fig. 4. Comparison between measured and calculated bi-directional spectra (450–2450 nm) for soil at site A (A) and B (B) for all treatments.

should also be removed from the measurements otherwise the retrieved values of the parameters might incorporate information on the soil bi-directional reflectance and the illumination conditions and hence would not be atmospherically invariant (Privette et al., 1995). However, the inclusion of an isotropic diffuse irradiance formulation added to the soil model of Jacquemoud et al. (1992) was found by Privette et al. (1995) to be of limited use. Diffuse irradiance was not included in the model used here and the measurement of reflectance on clear sky days was assumed to contribute little to the retrieved values of the bi-directional reflectance parameters. In hindsight, perhaps shading the target and measuring the bi-directional reflectance could have been used to test this assumption (pers. comm. anonymous reviewer).

The goniometer and radiometer were placed on the soil surface at exactly the same location in each plot after each treatment. The goniometer had a digital camera strapped to it so that images of the soil surface were also captured at each angle that reflectance was measured to provide a visual record of changes to the soil surface composition and structure during the experiments. As there were some problems with the camera, some images are missing. In addition, the radiometer malfunctioned partway through the experiment and a replacement was not made available until a month later. Whilst this hiatus curtailed the experiments, reflectance and imagery were measured once at each plot when the radiometer finally arrived.

2.7. Canonical ordination (redundancy analysis) of soil spectral reflectance

Redundancy analysis (RDA) was used here to establish the relations between model parameter values, sites (soil type) and treatment (Table 2). The technique was used by Chappell et al. (2005, 2006) to simplify the relationship between spectral reflectance changes with treatment. All aspects of the data analysis were identical to that used by Chappell et al. (2006) and readers interested in the details are referred to that publication.

3. Results

3.1. Soil surface characteristics and visual observations during treatments

Table 1 shows the surface (0–10 cm) properties of soil found in the vicinity (±150 m) of the field sites. These bulk soil

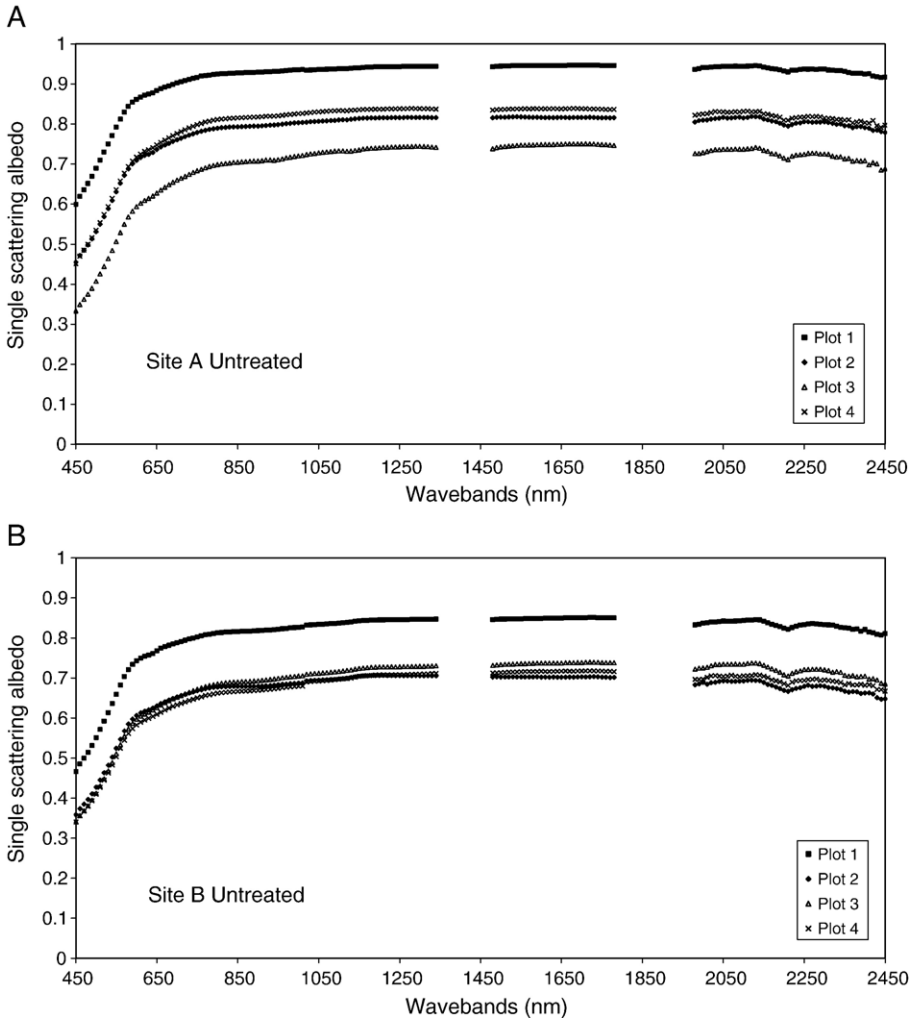

Fig. 5. The single scattering albedo (SSA) estimated using the bi-directional model of soil spectral reflectance for the untreated surface of soil at site A (A) and site B (B).

properties were measured as part of a larger project (Leys unpublished) performed two years previously, but as they are unlikely to change much from year to year they are used here to characterise the sites. Site B has slightly less clay and lower electrical conductivity (EC1:5) than Site A, but much larger amounts of salts (Cl, Na, Mg and Ca). These properties are indicative of larger soil salinity and potential for slaking of the soil surface; a process that makes the soil loose and friable, thus increasing the erodibility of Site B. These properties are consistent with field observations including digital images (Fig. 3), which show that site A had a massive, highly compacted soil, while the site B soil was less compacted and more friable, with a tendency to produce puffy surface structures. Site B had well developed biological soil crusts whilst site A showed no evidence of their presence.

The on-nadir images of selected soil surfaces at sites A and B, taken before and after each treatment, are shown in greyscale in Fig. 3. Due to problems with the camera some images are not available. Small elongate erosion features in the direction of abrasion are evident upon close inspection of the images (Fig. 3A) which increased the overall roughness. After non-ponding rainfall and natural drying (Fig. 3A, plot 1), the surface cracks are wider than before the treatment at plot 1. Vesicles and patches of fine red and brown material (dark in images) are also evident on plots 1 and 2 at this stage. The second abrasion of these plots had a greater impact than the first. Distinct elongate structures are typical of aeolian abrasion and increased the surface roughness of both plots. The major difference between the plots is that the coverage of abrasion is smaller in plot 1 than in plot 2. This is evident by the amount of underlying red material (dark in image) and the reduced coverage of the white green surface (lighter colours in image). After non-ponding rainfall, the surface of plot 2 returned to a mosaic of green/white (light shades) with patches of red/brown (dark shades). A month later without treatments the surface had lost the red/brown material (dark shades) and appears to be considerably lighter than the preceding images. This appears to be the case for the natural surface images from all plots at site A. Where the continuous rainfall was applied to the untreated soil surfaces (plots 3 and 4) the dried surfaces showed loose fragments. Abrasion of these plots produced elongate features across the surface similar to those produced during the second abrasion at plots 1 and 2. A second phase of high intensity

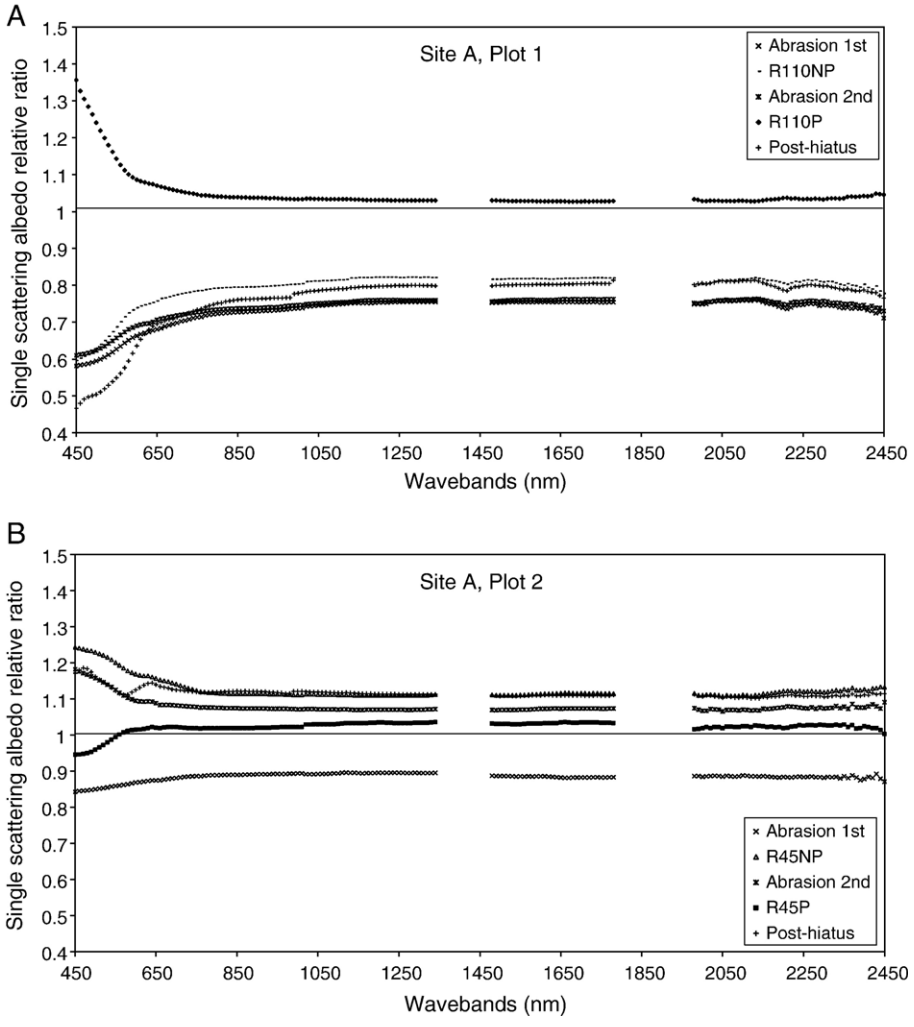

Fig. 6. The single scattering albedo (SSA) estimated using the bi-directional model of soil spectral reflectance for plot 1 (A), plot 2 (B), plot 3 (C) and plot 4 (D) divided by its untreated SSA spectra at site A.

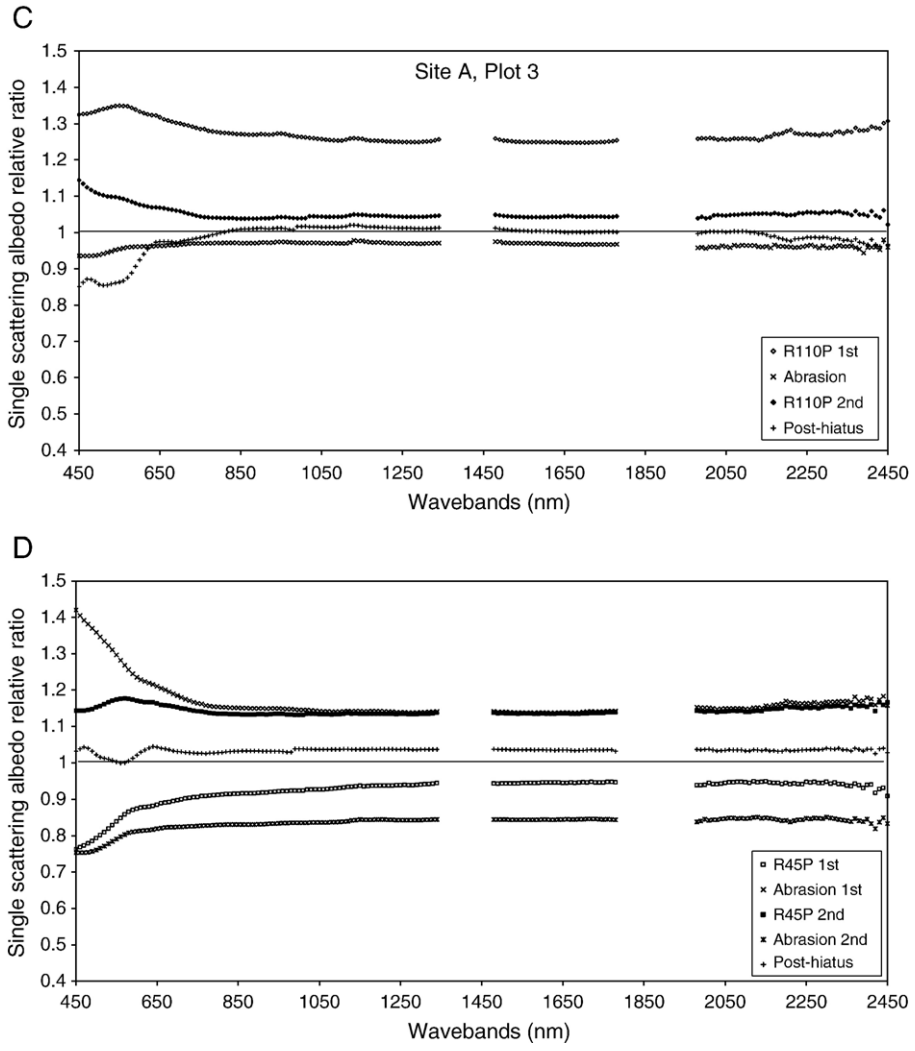

Fig. 6 (*continued*).

continuous rainfall on plot 3 produced a surface which was very smooth with well defined desiccation cracks. After a second phase of low intensity continuous rainfall the surface of plot 4 retained vestiges of the previous treatments in its surface roughness and the surface was far less cracked than plot 3.

The untreated surfaces at site B showed considerably more surface roughness than those at site A (Fig. 3B). This is a consequence of the soil properties and the larger amount of cyanobacteria than at site A but it is also because of the vestiges of the last rainstorm still evident in the soil surface (e.g., plot 4 untreated). At site B, untreated plots 1 and 2 were exposed to abrasion and the surface images showed vesicles and distinctly elongate features. Notably, the sizes of the features were much larger in their size and spacing and deeper than those aeolian abrasion features evident at site A. At plot 2 there were no vesicles evident and the abrasion features were much less extensive and the image showed that the central portion was largely intact. The images of plot 1 and 2 taken one month after the simulation experiments show the effect of the last treatments and natural processes. At plots 3 and 4, continuous rainfall was applied to the untreated surfaces. The image of plot 3 showed a very smooth surface whilst that for plot 4 appeared to have more surface roughness than the untreated surface (Fig. 3B). The image of the surface after abrasion showed vesicles and elongate features similar to those of plot 1 at this site.

3.2. Bi-directional (spectral) soil reflectance model

The model inversion procedure was stratified using site (soil type), plot and treatment. The optimised values of each model parameter for each site, plot and treatment and an assessment of accuracy are shown in Table 3. Fig. 4 shows the results of the measured spectra (450–2450 nm) at site A (Fig. 4B) and site B (Fig. 4B) against the calculated spectra for all treatments. The results showed a very good agreement (RMSE = 0.02) and plot along the 1:1 line.

The values of the bi-directional reflectance parameters represent the behaviour of the soil surfaces assuming that the soil reflectance model is appropriate and with the effect of reflectance sampling and illumination conditions removed. Notably, the scattering of light appears to be insensitive to the highly directional nature of the abrasion processes evident in the

images (Fig. 3A and B). In contrast, values of the *h* parameter appear to be sensitive to the treatments. In general, values of *h* were considerably larger (indicating smoother surfaces) for untreated soil surfaces or those treated with rainfall than those affected by abrasion. The values of *h* appear to identify the untreated surfaces of plots at site A as much smoother (larger values of *h*) than those at site B. In general, rainfall appeared to make the soil surfaces at both sites much smoother than the previous treatment. However, there were some plots in which rainfall caused the surface to become rougher than the previous treatment presumably as a consequence of the type of rainfall and the combination of antecedent conditions. It is these subtle changes in the soil surfaces which the canonical ordination was used to elucidate.

3.3. Single scattering albedo (SSA) spectra

Fig. 5 shows the single scattering albedo (SSA; ω) spectra for wavelengths between 450 nm and 2450 nm calculated by the model for both sites prior to any treatment. At site A the SSA spectra demonstrate that the soil surface of plots 2 and 4 are very similar to each other, but that of plot 1 has much larger SSA and plot 3 has much smaller SSA than that of plots 2 and 4 (Fig. 5A). Despite the difference in magnitude of SSA there appears to be little difference in the structure of the SSA. One exception is a tendency for the SSA at 2210 nm to be proportionally smaller at plot 3 than at other plots. The SSAs at site B are similar for plots 2, 3 and 4 but that at plot 1 is considerably larger than the others. The structure of the SSA for all plots at site B appears to be similar despite the difference in magnitude.

The SSA spectra for each treatment at each plot were divided by their respective spectrum for untreated soil at site A (Fig. 6A–D) and site B (Fig. 7A–D). The ratio reduced common and constant features and therefore enhanced differences in the spectra (Ben-Dor et al., 2003). The solid horizontal lines in Figs. 6 and 7 represent the SSA spectra of the untreated surfaces at sites A and B.

3.3.1. Site A

At site A, plot 1 (Fig. 6A) abrasion of the untreated surface reduced the magnitude of the SSA and produced the most significant differences in the visible (VIS ca. <1000 nm) region. Non-ponding high intensity rainfall (*R110NP*) increased the

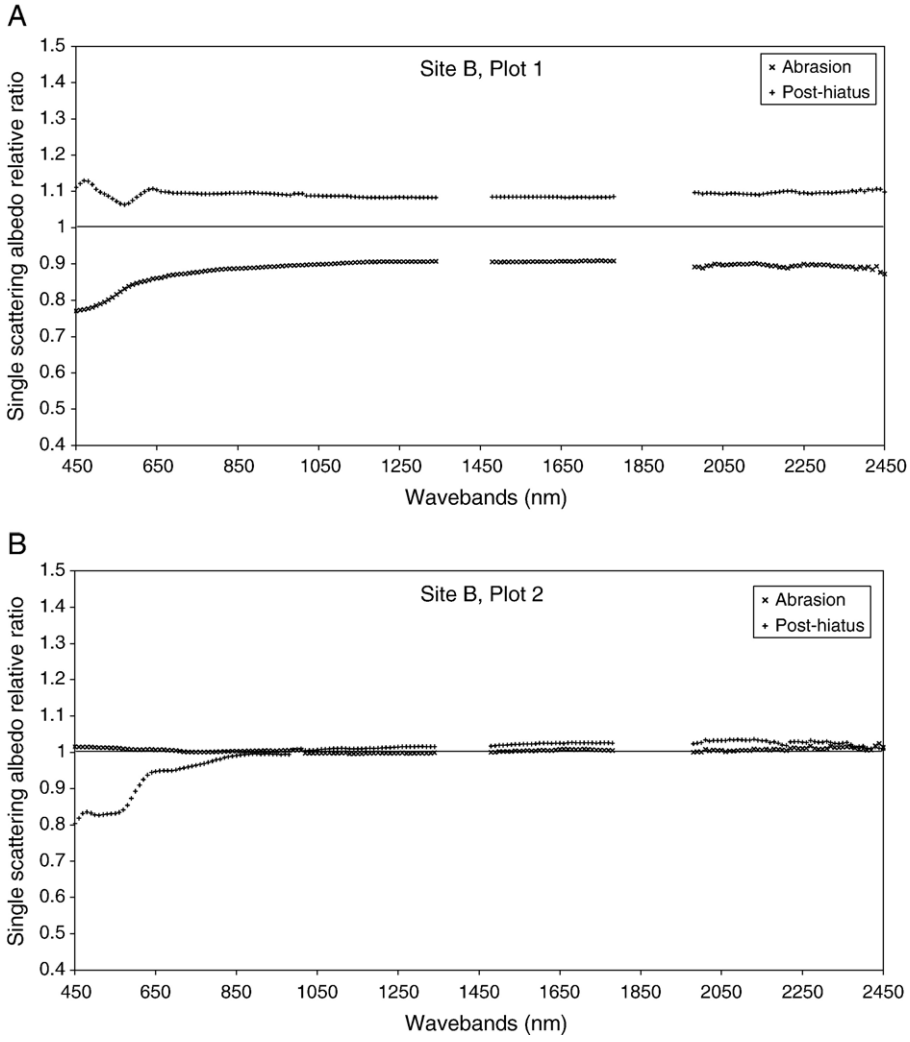

Fig. 7. The single scattering albedo (SSA) estimated using the bi-directional model of soil spectral reflectance for plot 1 (A), plot 2 (B), plot 3 (C) and plot 4 (D) divided by its untreated SSA spectra at site B.

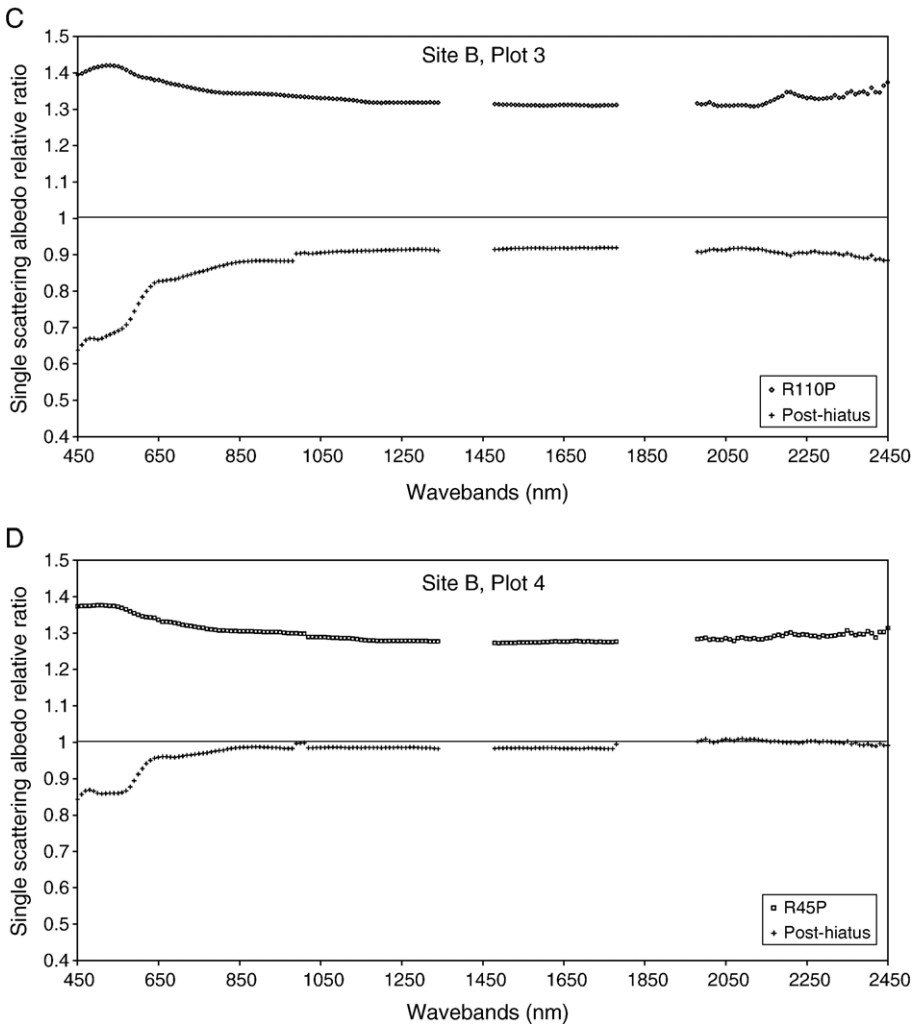

Fig. 7 (*continued*).

SSA in all but the smallest wavebands but did not return it to that level evident in the untreated state. The second abrasion treatment almost\raster(100%,p)=”figure7” reproduced the SSA in all wavebands that were evident after the initial abrasion. Wavebands smaller than ca. 820 nm had slightly larger SSA values than those produced after the first abrasion. The greatest difference amongst treatments for this plot was evident in the second rainfall simulation using ponding high intensity rainfall (*R110P*). In this case the SSA was generally much larger than that of the untreated surface and in particular the SSAs of wavebands less than ca. 790 nm were considerably larger than those of the untreated surface. The vestiges of soil treatments and the action of undefined natural processes reduced the SSA and introduced spectral features at 480 nm, 510 nm and 980 nm. These wavebands are well known for their association with haematite and goethite. Notably, the SSA spectrum obtained post-hiatus is the only one which crosses the abraded spectra.

At site A, plot 2 (Fig. 6B), the initial abrasion of the untreated surface reduced the magnitude of the SSA and produced the most significant differences in the VIS region. Non-ponding low intensity rainfall (*R45NP*) increased the SSA in all but the smallest wavebands but did not return it to that evident in the untreated state. In contrast to plot 1, the second abrasion treatment reduced the SSA in all wavebands relative to that of the *R45NP*. The second rainfall simulation *R45P* reduced the SSA to amounts very similar to those of the untreated surface. However, the SSA of wavebands less than ca. 560 nm was smaller than those of the untreated surface. Notably, the values of the wavebands less than ca. 570 nm obtained post-hiatus returned to the same levels as those of the second abrasion and *R45NP*.

At site A, plot 3 (Fig. 6C) high intensity ponding rainfall (*R110P*) was applied to the untreated surface. It produced a spectrum of SSA with values much larger than those for the untreated surface. Distinct spectral features were evident at ca. 560 nm and 2210 nm. Abrasion of that surface returned the spectra of SSA to values that were very similar to those for the untreated surface with perhaps slightly smaller values evident in the smallest wavebands. Another application of *R110P* caused the SSA spectra to be larger than that of the untreated surface. The greatest change appeared to take place once again in the smallest wavebands. The SSA spectrum obtained post-hiatus, crossed the abraded spectra at ca. 650 nm and displayed spectral features similar to those evident in other plots at the same time (Fig. 6).

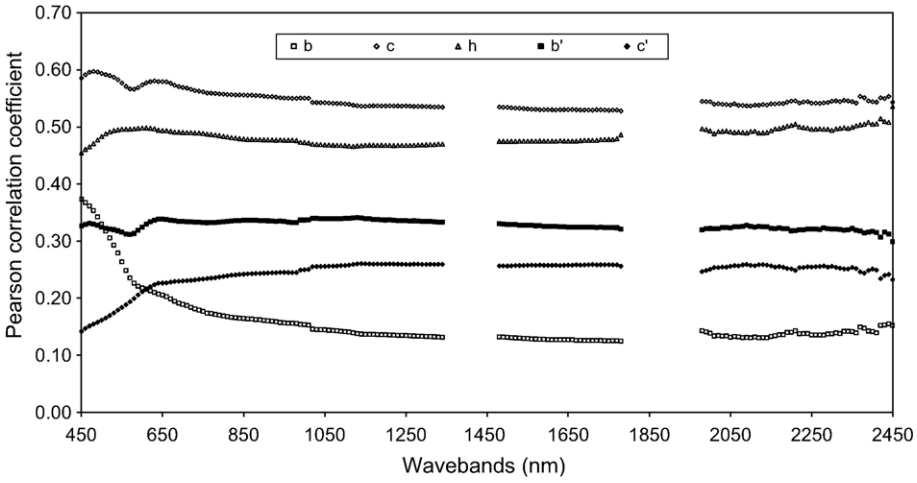

Fig. 8. Pearson correlation between each waveband and the retrieved parameter values of the bi-directional soil spectral reflectance model for each soil surface. These correlations were used to assist with the identification of wavebands used in the ordination analysis.

Low intensity ponding rainfall (*R45P*) was applied to the untreated surface. It produced a spectrum of SSA with values smaller than those of the untreated surface. The maximum deviation from the SSA spectrum occurred at wavelengths smaller than ca. 650 nm. A small spectral feature was evident at 650 nm. Abrasion of the surface decreased the SSA spectrum but retained spectral features at 650 nm and deepened the absorption at 490 nm and 2420 nm. The second application of *R45P* increased the SSA and introduced, relative to the spectrum of the untreated surface, a low round feature at ca. 560 nm. The second phase of abrasion appeared to change only those values in the VIS region of the SSA spectrum. The SSA spectrum obtained post-hiatus was very similar to that of the untreated surface. In addition spectral features were evident at ca. 460 nm, 560 nm and 990 nm.

3.3.2. Site B

At site B, plot 1 (Fig. 7A), abrasion of the untreated surface reduced the magnitude of the SSA and produced the most significant differences at wavelengths smaller than ca. 650 nm. The SSA spectrum obtained post-hiatus had values larger than those of the untreated surface and spectral features similar to those evident in the post-hiatus SSA spectrum for site A, plot 4. The abrasion of the untreated surface at site B, plot 2 (Fig. 7B) did not change the SSA spectrum. The post-hiatus SSA spectrum was also very similar to that of the untreated surface except in wavelengths in the VIS region in which spectral features similar to those evident in the post-hiatus SSA spectrum of site B plot 1.

At site B, plot 3 (Fig. 7C) *R110P* considerably increased the SSA spectrum relative to that of the untreated surface. The low round spectral feature at ca. 540 nm was evident and so too were features at 2010, 2210, 2360 and 2410 nm. The spectral features in the short-wave infrared (SWIR ca. 1800–2450 nm) region were much reduced in the post-hiatus SSA spectrum. However, those in the VIS region were greatly deepened and a new feature at 990 nm was evident in the spectrum. The spectra at site B, plot 4 (Fig. 7D) were very similar to those evident from plot 3 despite the application of *R45P*.

3.4. Canonical ordination (redundancy analysis)

Pearson correlation between each waveband and the retrieved parameter values of the bi-directional soil spectral reflectance model was used to assist with the identification of 15 wavebands used in the first ordination analysis (Fig. 8). The following wavebands were selected using a combination of spectral features, strong correlations obtained here, and wavebands known from previous research (e.g., Leone & Sommer, 2000) to be diagnostic: 450, 480, 580, 650, 850, 990, 1130, 1260, 1590, 2000, 2070, 2220, 2350, 2370, 2420 nm. The correlations also showed that the greatest amount of variation was evident in the VIS range of the wavebands. The largest correlation between reflectance parameter values and waveband SSA for each treatment appeared to be *c* followed closely by *h*. The correlations of the other parameters were below 0.4.

Preliminary ordination analyses with waveband SSA and using model parameter values showed that information from the untreated stage of the plots and from the final and much later reflectance measurements diminished the strength of the relationships and were removed from the final analyses described below.

The results of the redundancy analysis (RDA) between waveband SSA and the remaining soil treatments for both sites (A and B) are shown in Table 4. The eigenvalues measure the

Table 4
Ordinary redundancy analysis to explain the variation in selected wavebands and soil spectral model parameters using sites (soil type) and treatments

	Wavebands and treatments		Model parameters and treatments	
Axes	1	2	1	2
Eigenvalues	0.54	0.06	0.36	0.20
Waveband-treatment correlations	0.84	0.71	0.92	0.64
Cumulative percentage variance:				
Of waveband data	54.2	60.0	35.7	55.7
Of waveband-treatment relations	85.2	94.3	61.0	95.1

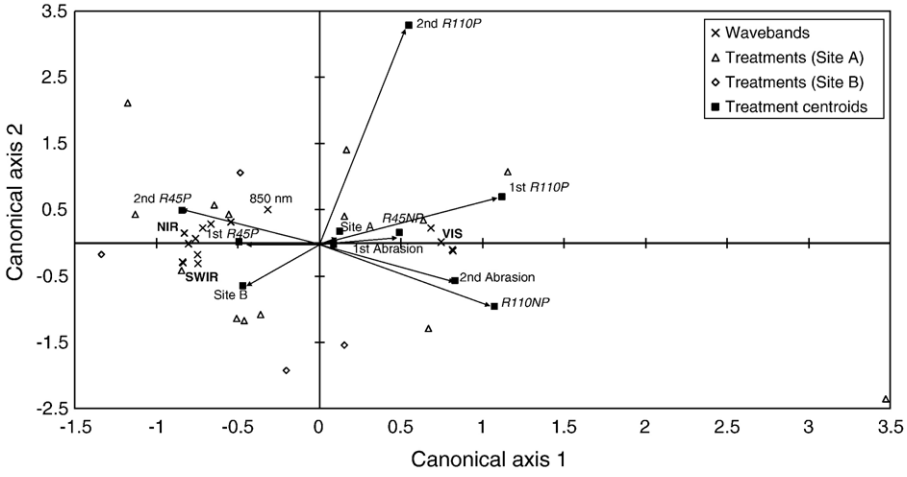

Fig. 9. Ordination diagram of redundancy analysis showing the relationships between wavebands and the ordination axes and the correlations between sites (soil types), plots and treatments and ordination axes.

importance of each of the canonical axes. The first axis explains 54% of the variation between the reflectance in each waveband and the treatments whilst the second axis explains only 6%. Thus, 60% of the variation in the data is explained by the first two axes. In addition, the relationship between the wavebands and the treatments for each axis is very strong. The amount of variation between the wavebands and the treatments is explained by each axis and is given as a cumulative percentage on the bottom line of Table 4. Approximately 85% of the variation is explained by the first axis, and the second axis provides only an additional 9%.

Fig. 9 provides a visual explanation for these statistics. The wavebands are separated into distinct groups oriented approximately along axis 1. The VIS wavebands are strongly related to the positive direction of axis 1, whilst those in the near-infrared (NIR ca. 1000–1800 nm) and SWIR are strongly related to the negative direction of the same axis. This axis is explained by the difference between discontinuous rainfall (largely regardless of the intensity) and continuous low intensity rainfall (*R45P*). Notably, the first abrasion is not important to the separation in the wavebands but the second abrasion is. Axis 2 is dominated by the second application of continuous high intensity rainfall (*R110P*) but the wavebands are not well distributed along it.

The results of the RDA between model parameters and the soil treatments for both sites (A and B) are also shown in Table 4. The first axis explains 36% of the variation between the values of the parameters and the treatments whilst the second axis explains 20%. Thus, 56% of the variation in the data is explained by the first two axes. Approximately 61% of the variation is explained by the first axis and the second axis provides an additional 34%. A visual explanation for these statistics is provided in Fig. 10. The model parameters are mainly distributed along axis 1. Parameters b and c' are aligned strongly with the first continuous application of low intensity rainfall (*R45P*). In contrast, parameters b', c and h are aligned with the negative direction of axis 1 which is associated with the first and second applications of continuous high intensity rainfall (*R110P*). Notably, the parameter h is almost exactly aligned with the first application of *R110P* suggesting that that treatment can be readily predicted by it. It appears that axis 1

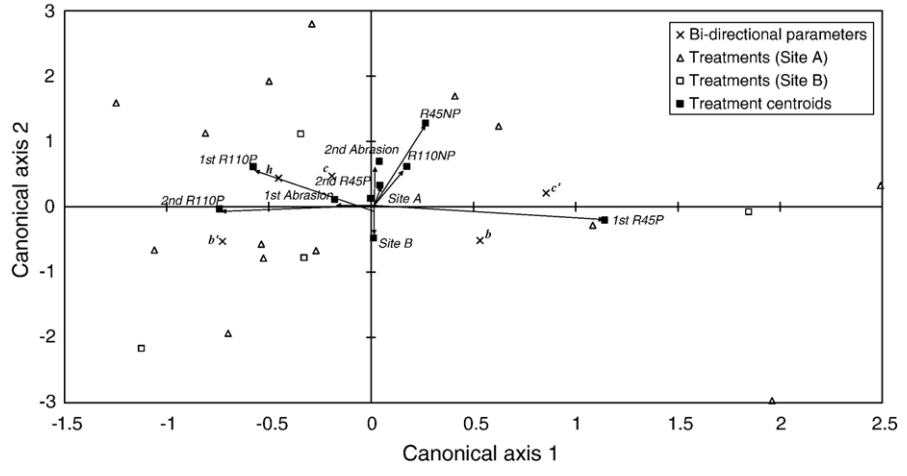

Fig. 10. Ordination diagram of redundancy analysis showing the relationships between bi-directional soil spectral model parameters and the ordination axes and the correlations between sites (soil types), plots and treatments and ordination axes.

separates the intensity of continuous rainfall. The orthogonal axis does not explain well the reflectance parameters and is dominated in the positive direction by the second abrasion and to a lesser extent that direction is explained by discontinuous rainfall of high and low intensity (*R110NP* and *R45NP*). The negative direction apparently separates site B from site A in terms of the responses to the treatment and is therefore associated with soil type.

4. Discussion

4.1. Soil surface properties

The study area used in the experiments described here was identified previously as particularly erodible. Since wind erosion was known *a priori* to be highly spatially and temporally variable (Chappell et al., 2003a,b), two sites were chosen to represent the surface conditions in the study area. It was evident from the soil properties at the two sites (Table 1) that the surface comprised very fine material. However, the erodibility of a soil surface, particularly by wind, is controlled by the composition and structure of the surface. The large amount of salts and the large electrical conductivity of the playa indicated a large amount of soil salinity which in turn causes slaking, a reduction in soil aggregation and a concomitant reduction in soil pore spaces and infiltration. Thus, the surface at site A was a thick, compact indurated layer with a smooth surface (Fig. 3A). At site B there were slightly larger amounts of silt and K and a smaller electrical conductivity than at site A. These properties, in addition to the presence of cyanobacteria, are believed to be responsible for the smooth, puffy biogenic crust and highly erodible condition of the surface at site B (Fig. 3B). However, it is not clear how the soil properties at site B are related to the surface erodibility and an explanation is also beyond the scope of this paper.

4.2. Variability of soil surface conditions

The single scattering albedo (SSA) removed the effect of viewing and illumination geometry on the spectra measured on the untreated and treated plots at both sites. Those SSA spectra of the untreated surfaces demonstrated the inherent variability of the soil surface condition within a site, despite the relatively small distances between plots (Fig. 5). The main difference amongst those untreated SSA spectra at site A occurred in plots 1 and 3 and at site B in plot 1. The difference between spectra appeared to be mainly in magnitude which might reasonably be ascribed to soil moisture. The lengthy drying period and highly evaporative conditions ensured consistently small amounts of moisture. However, variation in moisture may be caused by spatial variability, amongst the plots, of those soil properties that control the infiltration and retention of moisture (particle size, organic matter, biogenic crust etc.). Thus, within the approximately 10 m^2 site the soil properties that control soil moisture appear to be sufficiently variable to produce significantly different SSA spectra. The bi-directional soil spectral reflectance model parameter values appear to be diagnostic of the soil surface variability. The plots at site A had considerable variation in the roughness parameter h. That variation was much greater than the variation in h evident within the plots at site B. Notably, model parameter values for the untreated surface of plot 1 were considerably different from those of the other plots at site B and this difference was also evident in the scattering (Table 3).

It is difficult to assess the importance of the variability in the untreated surfaces on the subsequent behaviour of surfaces after treatment. However, consideration of the surface response to similar first treatments may provide some insight into its importance. Fig. 6A and B for site A, and Fig. 7A and B for site B, display the SSA spectra for the abrasion of plots 1 and 2. Fig. 6C and D show the SSA spectra of plots 3 and 4 treated similarly with *R110P*. It appears that the antecedent conditions played an important part in the soil surface response to abrasion at both sites. The magnitude of the SSA spectra was different at both sites and spectral features at 2210 nm and around 560 nm and 690 nm were evident in the spectra of one plot and not in the other, within sites. However, the values of the model parameters for initial abrasion at site A displayed very similar values in both cases. In contrast, the values of the model parameters for initial abrasion at plots 1 and 2 for site B were different in the values of h parameter. The images taken after these treatments support these findings (Fig. 3A and B). Specifically at site B, it is likely that difference in the surface of plots 1 and 2 evident after abrasion was due to a difference in the strength or the composition of the biogenic crust. The presence of a physical soil crust is well known to considerably effect the soil surface erodibility (Chappell et al., 2006; Goossens, 2004; Le Bissonais, 1990; Moore & Singer, 1990; Mualem et al., 1990; Zobeck, 1991a) and the strength of a crust has been shown to control the erosion rate (McKenna Neuman & Maxwell, 1999, 2002; McKenna Neuman et al., 1996; Rice & McEwan, 2001). Biological soil crusts are common in dryland environments (Belnap & Lange, 2003) and cyanobacterial crusts in particular are believed to significantly increase soil surface cohesion, total nitrogen and organic matter of the surface and change roughness (Campbell, 1979; Isichei, 1990; Malam Issa et al., 2001; Thomas & Dougill, in press). They have been shown to reduce soil surface erodibility to wind, because cyanobacterial filaments entangle surface particles (e.g. Belnap & Gillette, 1997, 1998; Thomas & Dougill, in press). However, a recent detailed study of the biological soil crusts at this field site (Strong, unpublished data) indicate that their relationship with erodibility is not so clear cut. The results presented here suggest that an assessment of soil surface erodibility must be made relative to the antecedent conditions and which vary temporally. This finding is particularly significant with a view to developing this work for a more operational remote sensing perspective. However, caution is required in the extrapolation of these findings because the application of rainfall, drying and subsequent abrasion of plots 1 and 2 changed considerably the visual characteristics (Fig. 3A), SSA spectra (Fig. 6A and B) and model parameter values (Table 3). Thus, the rainfall may represent a similar natural process that works to reset the soil surface conditions and in this case it may be the single most

important factor for considering the spatial and temporal variability in surface condition.

The variability considered above led to a comparison of the variability in soil surface response to treatments amongst sites. One of the most striking differences between the sites was the effects of abrasion on the untreated surfaces. As expected based on soil properties and surface observations, initial abrasion at site A changed the soil surface in a much smaller way than that of site B (Fig. 3A and D). Furthermore, the z_0 of plots 1 and 2 at site A showed little difference before and after *R110P* and were on average 0.0017 mm ($\sigma = 0.00016$). At site B, z_0 was an order of magnitude larger (plot 1 $z_0 = 0.02$ mm and plot 2 = 0.01 mm) than the surfaces at site A. However, there was no statistically significant correlation between any of the model parameter values and z_0. This is particularly surprising since the model parameter h is related to surface roughness. It appears that the model parameters, and h in particular, are not related to the scale of structures created by the rainfall simulation and wind tunnel abrasion but instead are sensitive to the particle size distribution at, or very near, the surface (Hapke, 1981). These results suggest that a correction for macroscopic roughness (e.g., Hapke, 1984) is required to investigate the scale of soil surface erodibility created by natural environmental processes.

4.3. Ordination analyses of wavebands and model parameters

It is evident from the above discussion that only the simplest experiments can be considered without recourse to a statistical analysis because of the interaction of antecedent conditions on the soil surface response to treatments. This was the basis of the approach used in previous analyses (Chappell et al., 2005, 2006). It was used here to consider separately the relationship between wavebands and treatments and between model parameters and treatments. This separation is consistent with our expectation that the wavebands contain information about the composition of the soil surface and therefore changes at the surface due to the treatments should be evident in the changes in the SSA spectra. Similarly, there should be a relationship between changes in the type and nature of light scattering as the soil surface responds to the treatments and hence the model parameters should represent those changes, notwithstanding the previously noted differences in scales between h and the affect of the treatments.

The ordination plot of the SSA wavebands and treatments against the first two ordination axes (Fig. 9) demonstrates the explanation of variance (60%) contained in the eigenvalues (Table 4). The first axis (54%) dominates the explanation and it separates SSA in wavebands in the VIS from those of the NIR and SWIR region. The exception to this pattern is the SSA at 850 nm which tends to follow that of the NIR. Although not strongly correlated, site A appears to be associated with SSA in wavebands in the VIS and site B seems to be associated with SSA in the SWIR. Regardless of how it was applied, high intensity rainfall (*R110NP* and *R110P*), is highly positively correlated with SSA in the VIS region and therefore negatively correlated with SSA in the other regions. Notably, the second abrasion is also highly positively correlated with SSA in the VIS and negatively correlated with reflectance in the NIR and SWIR. This apparently contradictory relationship is because of the interaction between abrasion intensity and prior rainfall. It also explicitly relates the increases in red (dark tone patches in Fig. 3A) clusters at the surface to increases in iron oxides commonly identified in the VIS region. Since the soils are prone to slaking there is a considerable amount of freely available iron which appears to be readily moved to the surface after high intensity rainfall. Abrasion strips away that surface material. However, the strong positive relationship between low intensity rainfall (*R45P*), again regardless of how it was applied, and SSA in the NIR and SWIR suggest that salts and clays (because of their demonstrated occurrence in this environment) are brought to the surface and subsequently removed by abrasion.

The ordination plot of the model parameter values and treatments against the first two ordination axes is shown in Fig. 10. The axes together explain approximately 60% of the variation which was similar to the previous analysis. Axis 1 explains 36% of the variation and is dominated by the ponding application of the rainfall regardless of the intensity (Table 4). Model parameters h, b' and to a less extent c are positively correlated with high intensity ponding rainfall (*R110P*; in the negative direction of axis 1) whilst the remaining model parameters (b and c') are positively correlated with low intensity ponding rainfall (45 mm h^{-1}; *R45P*). The scattering is evidently mixed in its association with these treatments and little more information about the diffuse and specular nature of the scattering can be extracted. It appears that as high intensity rainfall increases, h increases, which would be consistent with the surface becoming smooth, and for the development of a surface crust. The first application of low intensity ponding rainfall (*R45P*) is negatively correlated with h suggesting that the surface tends to become rough. Remembering the microscopic scale of the h parameter, these results suggest that *R45P* has reduced the surface roughness. This finding is consistent with the previous ordination analysis of wavebands and treatments that suggested salts and clays were brought to the surface either during rainsplash or more probably during intense evaporation at the surface. The implication is that high intensity ponding rainfall sealed the surface and did not allow eluviation of salts. Furthermore, low intensity ponding rainfall created a crust that facilitated the eluviation of salts/clays to the surface which decreased the microscopic roughness. The positive direction of axis 2 is explained by abrasion, in particular the second abrasion, to non-ponding rainfall, regardless of the intensity, and to a much less extent by those treatments at site A. In contrast, the negative direction of axis 2 is explained almost solely by treatments performed at site B. This axis is clearly associated with a scale of roughness much larger than that of h because the images of these surfaces show evidence of rain drop impacts and aeolian abrasion features (Fig. 3A and B).

5. Summary and conclusions

A claypan (playa) in south western Queensland, Australia well known for wind erosion and dust production, was used for

this study. The area is exposed to highly evaporative conditions and sporadic inundation by water from the nearby Diamantina River. Consequently, the soil surface comprised very fine material, large amounts and different types of salts, large electrical conductivity and a propensity for slaking. The soil surface of two sites (A and B) on the playa was modified using *in situ* rainfall simulation and wind tunnel abrasion experiments. At site A the surface was a thick, compact indurated layer with a smooth surface. The surface at site B was also smooth but puffy in the presence of a biogenic crust and appeared highly erodible. Changes of the soil surfaces were recorded using digital images and multi-angular spectral measurements of reflectance and inverted against a bi-directional soil spectral reflectance model. An assessment of the performance of the model calculation relative to the measurements for each site showed good agreement with small acceptable variation in accuracy. Optimised values of the model parameters produced the single scattering albedo (SSA) and a description of the scattering behaviour of the soil surfaces that included an estimate of microscopic roughness. The model parameters removed the effect of the measurement conditions (illumination and viewing geometry) on the spectral reflectance.

Four plots were chosen within approximately 10 m^2 at each site for application of the treatments. The SSA spectra and the model parameter values of the untreated surfaces were examined before and after initial abrasion to make a preliminary assessment of the extent to which variability in the surface conditions at this scale would influence the outcome of the treatments. It appeared that subtle differences in the factors controlling soil moisture (e.g., particle size, soil porosity etc.) were sufficiently variable to produce significant differences in the SSA spectra. These differences were identified by the model parameter values and appeared sensitive to the soil surface variability. Abrasion demonstrated that the variability in the surface conditions of the untreated surfaces played an important role in the response. These results suggested that an assessment of soil surface erodibility should be made relative to the antecedent surface conditions and which varied temporally. This finding is significant with a view to developing this work for a more operational and remote sensing perspective. However, caution is required in the extrapolation of these findings because the application of rainfall, drying and subsequent abrasion changed considerably the visual characteristics, SSA spectra and model parameter values. Thus, the rainfall treatment appeared to represent a natural process that reset the soil surface conditions and controlled the spatial and temporal variation in the soil surface conditions.

Redundancy analyses (RDA) were conducted separately for SSA of selected wavebands, model parameter values and treatments to elucidate the subtle and interactive effects not evident from straightforward comparisons. The analysis was performed on the basis that the wavebands contained information about the composition of the soil surface and changes at the surface due to the treatments would be evident in differences of the SSA spectra. Similarly, a relationship was expected between changes in the type and nature of light scattering as the soil surface responded to the treatments, particularly the directional nature of the abrasion process, and that the model parameter values would represent those changes assuming the model was appropriate. RDA separately of the SSA wavebands, model parameters and treatments explained 60% of the variation. The waveband and treatment RDA was dominated by one axis that was explained by the intensity of rainfall regardless of the nature of its application. The model parameters and treatments RDA was also dominated by one axis which was explained by the ponding application of the rainfall regardless of its intensity. High intensity rainfall and abrasion was associated with wavebands in the visible (VIS) region and an increase in h (reduced roughness). Low intensity rainfall was associated with wavebands in the near-infrared (NIR) and short-wave infrared (SWIR) regions and a decrease in h (increased roughness). This pattern was interpreted as the result of eluviation due to rainsplash impact which caused size segregation and the preferential translocation of iron oxides to the surface and the creation of a thick surface seal and caused a thin crust which enabled the movement of salts and/or mineral clays to the surface because of the strong evaporation gradient.

Considerable variation in the surface roughness between plots and sites was identified using digital imagery and estimates of aerodynamic resistance (z_0). Differences in roughness were caused by abrasion and its coincidence with other treatments as described above. For example, surfaces at site B exposed to abrasion had values of z_0 which were an order of magnitude larger than all surfaces treated similarly at site A. However, the bi-directional soil spectral reflectance model parameter h was not sensitive to these major changes. Instead it identified changes in microscopic surface roughness typically associated with particle size, porosity and density and hence was highly sensitive to surface seals and crusts. The results suggest that a correction for macroscopic roughness is required to investigate larger features of soil surface erodibility created by natural environmental processes such as rainsplash and wind erosion.

Acknowledgements

This work was funded by an award to AC from the UK Natural Environmental Research Council (NER/M/S/2001/00124). We are grateful to G. Brunner for technical assistance with the directional reflectance measurements and to S. Heidenrich for technical assistance with the operation of the wind tunnel. Assistance from S. Jacquemoud with the bi-directional soil spectral reflectance model and support from P. Lewis is also gratefully acknowledged. The comments of three anonymous reviewers were gratefully received. Any omissions or inaccuracies that remain in the paper are the sole responsibility of the authors.

References

Baumgardner, M. F., Silva, L. F., Biehl, L. L., & Stoner, E. R. (1985). Reflectance properties of soils. *Advances in Agronomy*, *38*, 1−44.

Belnap, J., & Gillette, D. A. (1997). Disturbance of biological soil crusts: Impacts on potential wind erodibility of sandy desert soils in southeastern Utah. *Land Degradation and Development*, *8*, 355−362.

Belnap, J., & Gillette, D. A. (1998). Vulnerability of desert biological soil crusts to wind erosion: The influences of crust development, soil texture, and disturbance. *Journal of Arid Environments*, *39*, 133−142.

Belnap, J., & Lange, O. L. (2003). *Biological soil crusts: Structure, function and management.* Berlin: Springer-Verlag.

Ben-Dor, E., Irons, J. R., & Epema, G. (1999). Soil reflectance. In A. N. Renzc (Ed.), *Remote sensing for the Earth Sciences*, *vol. 3* (pp. 111-188). New York: Wiley.

Ben-Dor, E., Goldshleger, N., Benyamini, Y., Agassi, M., & Blumberg, D. G. (2003). The spectral reflectance properties of soil structural crust in the 1.2 to 2.5 mm spectral region. *Soil Science Society American Proceedings*, *67*, 289−299.

Böhner, J., Schäfer, W., Conrad, O., Gross, J., & Ringeler, A. (2003). The WEELS model: Methods, results and limitations. *Catena*, *52*(4), 289−308.

Butler, H. J., McTainsh, G. H., Hogarth, W. L., & Leys, J. F. (2005). Kinky profiles: Effects of soil surface heating upon vertical dust concentration profiles in the Channel Country of western Queensland, Australia. *Journal of Geophysical Research*, *110*, F04025. doi:10.1029/2004JF000272

Campbell, S. E. (1979). Soil stabilization by a prokaryotic desert curst: Implications for Precambrian land biota. *Origins of Life*, *9*, 335−348.

Chappell, A., McTainsh, G., Leys, J., & Strong, C. (2003). Simulations to optimise sampling of aeolian sediment transport for mapping in space and time. *Earth Surface Processes and Landforms*, *28*, 1223−1241.

Chappell, A., McTainsh, G., Leys, J., & Strong, C. (2003). Using geostatistics to elucidate temporal change in the spatial variation of aeolian sediment transport. *Earth Surface Processes and Landforms*, *28*, 567−585.

Chappell, A., Zobeck, T., & Brunner, G. (2005). Induced soil surface change detected using on-nadir spectral reflectance to characterise soil erodibility. *Earth Surface Processes and Landforms*, *30*(4), 489−511.

Chappell, A., Zobeck, T., & Brunner, G. (2006). Using bi-directional soil spectral reflectance to model soil surface changes induced by rainfall and wind-tunnel abrasion. *Remote Sensing of Environment*, *102*(3–4), 328−343.

Cierniewski, J. (1987). A model for soil surface roughness influence on the spectral response of bare soils in the visible and near-infrared range. *Remote Sensing of Environment*, *23*, 97−115.

Dong, Z., Liu, X., & Wang, X. (2002). Aerodynamic roughness of gravel surfaces. *Geomorphology*, *43*(1−2), 17−31.

Fryrear, D. W., Saleh, A., Bilbro, J. D., Schomberg, H. M., Stout, J. E., & Zobeck, T. M. (1998). Revised Wind Erosion Equation (RWEQ). Wind Erosion and Water Conservation Research Unit, USDA-ARS, Southern Plains Area Cropping Systems Research Laboratory. Technical Bulletin No. 1. http://www.csrl.ars.usda.gov/wewc/rweq.htm

Geeves, G. W., Leys, J. F., & McTainsh, G. H. (2000). Soil erodibility. In P. E. Charman & B. Murphy (Eds.), *Soils their properties and management* (pp. 205−220). New York: Oxford University Press.

Goossens, D. (2004). Effect of soil crusting on the emission and transport of wind-eroded sediment: Field measurements on loamy sandy soil. *Geomorphology*, *58*, 145−160.

Hapke, B. W. (1963). A theoretical photometric function for the lunar surface. *Journal of Geophysical Research*, *68*, 4571−4586.

Hapke, B. W. (1981). Bidirectional reflectance spectroscopy 1. Theory. *Journal of Geophysical Research*, *86*, 3039−3054.

Hapke, B. W. (1984). Bidirectional reflectance spectroscopy. 3. Correction for macroscopic roughness. *Icarus*, *59*, 41−59.

Huete, A. R., & Escadafal, R. (1991). Assessment of biophysical soil properties through spectral decomposition techniques. *Remote Sensing of Environment*, *35*, 149−159.

Isichei, A. O. (1990). The role of algae and cyanobacteria in arid lands. A review. *Arid Soil Research and Rehabilitation*, *4*, 1−17.

Jacquemoud, S., Bater, F., & Hanocq, J. F. (1992). Modeling spectral and bidirectional soil reflectance. *Remote Sensing of Environment*, *41*, 123−132.

Latz, K. R. A., Weismiller, G. E., Van Scoyoc, G. E., & Baumgardner, M. F. (1984). Characteristic variations in spectral reflectance of selected eroded Alfisols. *Soil Science Society of America Journal*, *48*, 1130−1134.

Le Bissonais, Y. (1990). Experimental study and modelling of soil surface crusting processes. In R. B. Bryan (Ed.), *Soil erosion—Experiments and models Catena Supplement*, *vol. 17 (pp. 13–18).*

Leone, A. P., & Sommer, S. (2000). Multivariate analysis of laboratory spectra for the assessment of soil development and soil degradation in the southern Apennines (Italy). *Remote Sensing of Environment*, *72*, 346−359.

Leys, J. F., & Raupach, M. R. (1991). Soil flux measurements using a portable wind erosion tunnel. *Australian Journal of Soil Research*, *29*, 533−552.

Mahowald, N., Bryant, R. G., del Corral, J., & Steinburger, L. (2003). Ephemeral lakes and desert dust sources. *Geophysical Research Letters*, *30* (2), 1074−1078.

Malam Issa, O., Le Bissonnais, Y., Defarge, C., & Trichet, J. (2001). Role of a cyanobacterial cover on structural stability of sandy soils in the Sahelian part of western Niger. *Geoderma*, *101*, 15−30.

Marticorena, B., & Bergametti, G. (1995). Modeling the atmospheric dust cycle: 1. Design of a soil-derived dust emission scheme. *Journal of Geophysical Research*, *100*(D8), 16, 415−16, 430.

McKenna Neuman, C., & Maxwell, C. D. (1999). A wind tunnel study of the resilience of three fungal crusts to particle abrasion during aeolian sediment transport. *Catena*, *38*, 151−173.

McKenna Neuman, C., & Maxwell, C. D. (2002). Temporal aspects of the abrasion of microphytic crusts under grain impact. *Earth Surface Processes and Landforms*, *27*, 891−908.

McKenna Neuman, C., Maxwell, C. D., & Boulton, J. W. (1996). Wind transport of sand surfaces crusted with photoautotrophic microorganisms. *Catena*, *27*, 229−247.

McTainsh, G. H., Leys, J. F., & Nickling, W. G. (1999). Wind erodibility of arid lands in the Channel Country of western Queensland, Australia. *Zeitschrift für Geomorphologie Supplementband*, *116*, 113−130.

Moore, D., & Singer, M. (1990). Crust formation effects on soil erosion processes. *Soil Science Society of America Journal*, *54*(4), 1117−1123.

Morin, J., Goldberg, D., & Seginer, I. (1967). A rainfall simulator with a rotating disc. *Trans American Society Agricultural Engineers*, *10*, 74−77.

Mualem, Y., Assouline, S., & Rohdenburg, H. (1990). Rainfall induced soil seal. (A) A critical review of observations and models. *Catena*, *17*(2), 185−203.

Nickling, W. G., McTainsh, G. H., & Leys, J. F. (1999). Dust emissions from the Channel Country of western Queensland, Australia. *Zeitschrift für Geomorphologie Supplementband*, *116*, 1−17.

Pinty, B., Verstraete, M. M., & Dickinson, R. E. (1989). A physical model for predicting bidirectional reflectances over bare soil. *Remote Sensing of Environment*, *27*, 273−288.

Privette, J. L., Myneni, R. B., Emery, W. J., & Pinty, B. (1995). Inversion of a soil bidirectional reflectance model for use with vegetation reflectance models. *Journal of Geophysical Research*, *100*(D12), 25497−25508.

Rice, M. A., & McEwan, I. K. (2001). Crust strength: A wind tunnel study of the effect of impact by saltation particles on cohesive soil surfaces. *Earth Surface Processes and Landforms*, *26*, 721−733.

Seubert, C. E., Baumgardner, M. F., & Weismiller, R. A. (1979). Mapping and estimating aerial extent of severely eroded soils of selected sites in Northern Indiana. *Institute of Electrical and Electronic Engineers*, 234−239.

Shao, Y., & Leslie, L. M. (1997). Wind erosion prediction over the Australian continent. *Journal of Geophysical Research*, *102*(D25), 30091−30105.

Shao, Y., McTainsh, G. H., Leys, J. F., & Raupach, M. R. (1993). Efficiencies of sediment samplers for wind erosion measurement. *Australian Journal of Soil Research*, *31*(4), 519−532.

Shao, Y., Raupach, M. R., & Leys, J. F. (1996). A model for prediction of aeolian sand drift and dust entrainment on scales from paddock to region. *Australian Journal of Soil Research*, *34*, 309−342.

Sokolik, I. N., & Toon, O. B. (1996). Direct radiative forcing by anthropogenic airborne mineral aerosols. *Nature*, *381*, 681−683.

Stoner, E. R., & Baumgardner, M. F. (1981). Characteristic variations in reflectance of surface soils. *Soil Science Society of America Journal*, *45*, 1161−1165.

Thomas, A. D., & Dougill, A. J. (in press). Spatial and temporal distribution of cyanobacterial soil crusts in the Kalahari: implications for soil surface properties. *Geomorphology.* doi:10.1016/j.geomorph.2006.03.029

Zender, C. S., Bian, H., & Newman, D. (2003). Mineral Dust Entrainment And Deposition (DEAD) model: Description and 1990s dust climatology. *Journal of Geophysical Research*, *108*(D14), 4416. doi:10.1029/2002JD002775

Zobeck, T. M. (1991). Abrasion of crusted soils: Influence of abrader flux and soil properties. *Soil Science Society American Proceedings*, *55*, 1091−1097.

Zobeck, T. M. (1991). Soil properties affecting wind erosion. *Journal of Soil and Water Conservation*, *46*(2), 112−118.